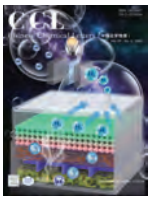
Chinese Chemical Letters 37 (2026) 111743

Contents lists available at ScienceDirect

Chinese Chemical Letters

journal homepage: www.elsevier.com/locate/cclet



Unveiling the role of Fe in natural tourmaline to tune the polarization field for hydrogen peroxide synthesis under ambient conditions

Huiru Chen[a], Zhi Li[a,*], Jingyi Yang[a], Li Gong[b,*], Mingshan Zhu[a]

[a] Guangdong Engineering Technology Research Center of Water Treatment Processes and Materials, College of Environment and Climate, Jinan University, Guangzhou 511443, China
[b] Instrumental Analysis Research Center, Sun Yat-sen University, Guangzhou 510275, China

ARTICLE INFO

Article history:
Received 21 May 2025
Revised 30 July 2025
Accepted 19 August 2025
Available online 20 August 2025

Keywords:
Piezocatalysis
H_2O_2 synthesis
Tourmaline
Polarization

ABSTRACT

Piezocatalysis offers an efficient approach for producing H_2O_2, a sustainable fuel and oxidant with a wide range of applications. Natural tourmaline, known for its exceptional piezoelectric properties, stands out as a promising green catalyst compared to other synthetic catalysts. In this study, natural tourmaline was modified using a simple acid treatment to remove iron, achieving effective piezocatalytic H_2O_2 synthesis at a rate of 513.7 μmol g^{-1} h^{-1} under ambient conditions. In-depth studies demonstrated that the Fe-free tourmaline exhibited a stronger polarization electric field due to the enhanced polyhedron distortion, compared to the Fe-containing tourmaline. The influence of temperature on their piezoresponse was also investigated. This study provides new insights into the mechanisms of piezoelectric H_2O_2 production using natural tourmaline.

© 2026 Published by Elsevier B.V. on behalf of Chinese Chemical Society and Institute of Materia Medica, Chinese Academy of Medical Sciences.

Hydrogen peroxide (H_2O_2) is an economical, eco-friendly fuel and oxidizer with diverse application scenarios [1–3]. As H_2O_2 demand surges, a significant supply-demand gap has emerged. Traditional H_2O_2 synthesis relies on the energy-intensive and environmentally harmful anthraquinone oxidation process [4]. There is an urgent need to explore sustainable and efficient alternatives for H_2O_2 production. Piezocatalysis has emerged as a promising technique for H_2O_2 synthesis, leveraging mechanical energy, such as sound, waves, and vibrations, to drive chemical reactions [5,6]. Piezoelectric effect originates from the properties of non-centrosymmetric piezoelectric materials [7]. When external strain is applied to the piezoelectric materials in a certain direction, polarization occurs in the materials, generating a localized electric field [8]. The magnitude of the polarization electric field is a critical factor that influence the efficiency of piezo-catalytic reactions [9,10]. Specifically, the polarization-induced charges serve as essential driving forces for the $2e^-$ oxygen reduction reaction (ORR) and water oxidation reaction (WOR), both of which are rate-limiting steps in H_2O_2 production [5,11,12]. Therefore, it is vital to modulate the polarization electric field of piezoelectric materials, thereby optimizing the generation and distribution of localized piezo-charges.

Studies on piezoelectric catalysts have predominantly focused on synthetic materials like ZnO, MoS_2, and $BiOIO_3$ [13–15]. However, synthetic materials often face challenges such as high production costs and limited commercial viability. In contrast, natural mineral materials like tourmaline offer significant advantages due to their cost-effectiveness, environmental friendliness and exceptional piezoelectric properties, making them highly promising for sustainable applications [9,16]. To date, piezocatalytic tourmalines have been applied in environmental field including dye decomposition, heavy metals adsorption, microorganism disinfection and Fenton-like processes [9,17–20]. The crystal structure of tourmalines is composed of XO_9 polyhedra, YO_6 octahedra and ZO_6 octahedra (where $X = Na^+$, Ca^{2+}, K^+ and vacancy, $Y = Mg^{2+}$, Fe^{2+}, Al^{3+}, *etc.*, $Z = Al^{3+}$, Fe^{3+}, Mg^{2+}, *etc.*), ring of six corner-sharing TO_4 tetrahedra ($T = Si^{4+}$), BO_3 trigon and anions (OH^-, O^{2-}, *etc.*) [21]. Previous studies showed that cationic distribution in Y octahedral position could influence its polarization electric field, further enhancing its catalytic efficiency [22], while Fe was considered as the main factor that affected the polarization of tourmalines [23]. However, the role of Fe in modulating the piezoelectric behavior of tourmalines and its subsequent impact on the generation of H_2O_2 remains ambiguous.

Herein, we investigated the piezoelectric catalytic effect of two different tourmalines including Fe-rich tourmaline (Fe-rich TM) and Fe-free tourmaline (Fe-free TM) for H_2O_2 production at ambient condition. Specifically, the Fe-free TM was simply derived

* Corresponding authors.
E-mail addresses: zhili@jnu.edu.cn (Z. Li), gongli2@mail.sysu.edu.cn (L. Gong).

https://doi.org/10.1016/j.cclet.2025.111743
1001-8417/© 2026 Published by Elsevier B.V. on behalf of Chinese Chemical Society and Institute of Materia Medica, Chinese Academy of Medical Sciences.

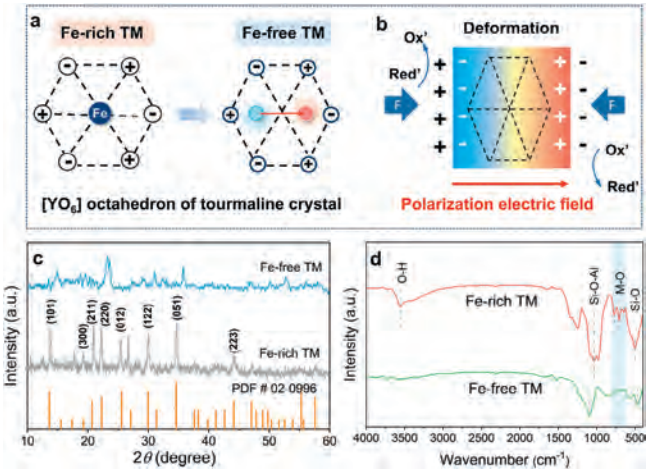


Fig. 1. Scheme of (a) polyhedron distortion and (b) the polarization electric field in two natural tourmalines. (c) XRD patterns and (d) FT-IR spectra of Fe-free TM and Fe-rich TM.

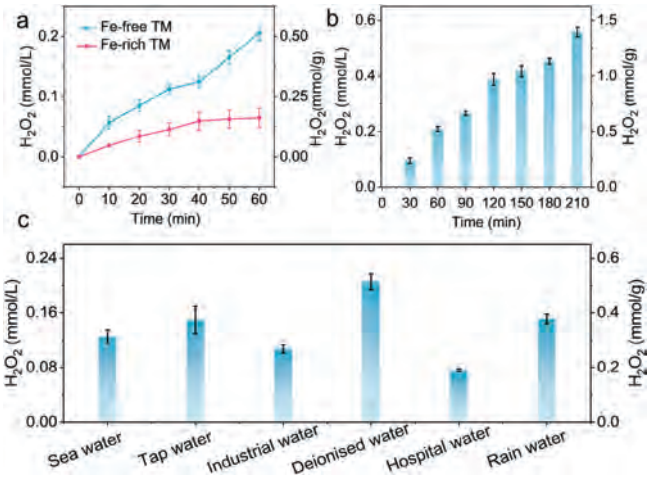


Fig. 2. (a) Piezocatalytic H_2O_2 production by Fe-free TM and Fe-rich TM. (b) Piezocatalytic H_2O_2 production over Fe-free TM under varying reaction times. (c) Piezocatalytic H_2O_2 production in different water samples after 60 min. Experimental conditions: Catalysts dosage = 0.4 g/L, ultrasonic power = 100 W, temperature = 25 °C.

from Fe-rich TM by hydrochloric acid pickling. As demonstrated in Fig. 1a, the removal of Fe in YO_6 octahedra lead to polyhedron distortion of the crystal structure, thereby improving the piezoelectric properties of TM. The abundant localized piezo-charges driven by the enhanced polarization electric field was utilized for the redox processes (Fig. 1b). The piezocatalytic H_2O_2 production rate was 513.7 μmol g^{-1} h^{-1} on Fe-free TM, which was three times higher than that of Fe-rich TM (161.1 μmol g^{-1} h^{-1}). The piezoelectric properties and polarization electric field of Fe-free TM were found to be superior to Fe-rich TM, as revealed by piezoresponse force microscopy (PFM) and zeta potential analysis, respectively. We also investigated the reaction pathway of H_2O_2 production using electron paramagnetic resonance (EPR), chemical probes and scavengers [24,25]. Moreover, the temperature-dependent PFM was conducted to analyse the correlation between temperature and piezoelectric coefficient (d_{33}). This study is expected to provide crucial insights into the mechanisms of piezoelectric H_2O_2 production by natural tourmaline, highlighting the impact of Fe on catalytic efficiency.

The structural and morphological properties of Fe-free TM and Fe-rich TM were characterized by scanning electron microscope (SEM) and X-ray diffraction (XRD) patterns. The SEM images revealed that both Fe-free and Fe-rich TMs consist of nonuniform micron-scale granular particle, with average diameter of 3.131 μm and 3.570 μm, respectively. The energy dispersive X-ray spectroscopy (EDS) results of Fe-free TM indicated the absence of Fe, whereas Fe-rich TM contained Fe at a proportion of 2.3 % (Figs. S1 and S2 in Supporting information). The XRD pattern of Fe-rich TM was well-indexed to tourmaline (PDF #02–0996). The crystallinity in Fe-free TM was reduced as shown in Fig. 1c, which indicated the destruction of the crystal structure. The chemical bond features of TMs were analyzed by Fourier transform infrared spectroscopy (FT-IR) (Fig. 1d). In the Fe-rich TM, peaks at 655 cm^{-1}, 715 cm^{-1} and 780 cm^{-1} were attributed to the stretching of M-O (M = Fe, Al, Mg), while the peak at 1042 cm^{-1} was assigned to O-Si-O stretching [26]. Another peak of Fe-rich TM at 509 cm^{-1} corresponded to the bending vibration of Si-O [27]. In the Fe-free TM, red shifts of the Si-O and Si-O-Al peaks to 474 cm^{-1} and 1107 cm^{-1} were observed, which were due to the variation of bond length and the reduction in bond energy, suggesting the crystal deconstruction in Fe-free TM [18]. Additionally, the absence of peaks associated with Fe in Fe-free TM confirmed the removal of Fe in YO_6 octahedra which agreed with the results shown in EDS results, survey X-ray photoelectron spectrometer (XPS) spectra (Fig. S3 in Supporting information) and Fe 2p high-resolution spectra of Fe-free TM (Fig. S4 in Supporting information). As depicted in Figs. S5 and S6 (Supporting information), the high-resolution O 1s XPS spectra of both TM deconvoluted into three distinct peaks. The peak at 530.3 eV corresponded to lattice O of tourmaline while the peaks at approximately 531.5 eV and 532.5 eV were attributed to bridging and the terminal hydroxyl group, respectively [18].

The piezoelectric performance of Fe-free TM and Fe-rich TM was subsequently evaluated under ultrasonic (Us) vibration. Control experiments without ultrasound showed no H_2O_2 production for either sample, confirming the essential role of piezoelectric effect (Fig. S7 in Supporting information). As shown in Fig. 2a and Fig. S8 (Supporting information), the H_2O_2 production rate reached 513.7 μmol g^{-1} h^{-1} on Fe-free TM under Us condition, surpassing Fe-rich (161.1 μmol g^{-1} h^{-1}) TM by three times and outperforming most reported synthetic piezo-catalysts. To further assess the feasibility of the Fe-free TM/Us system, experiments were conducted under various conditions. The results shown that H_2O_2 yield increased with the reaction time (0–210 min) (Fig. 2b) and the ultrasound power (20–100 W) (Fig. S9 in Supporting information). In addition, the variation of pH (pH 1, 4, 7, 9, 11) and catalysts amount (0.2–1 g/L) led to a volcanic trend of H_2O_2 production (Figs. S10 and S11 in Supporting information). The piezocatalytic H_2O_2 production performance of Fe-free TM remained stable over four cycles as shown in Fig. S12 (Supporting information). To explore the practical application, diverse real water samples comprising seawater, tap water, industrial wastewater, hospital effluent and rainwater were tested for piezoelectric H_2O_2 production using Fe-free TM. The aqueous samples displayed marginally reduced efficacy compared to pure water, which was attributed to the coexistence of ionic contaminants and dissolved organic compounds. (Fig. 2c).

The polarization electric field, with a strength ranging from 10^4–10^7 V/m, was generated on the surface of the TM due to its intrinsic electric dipole moment [28]. A stronger electric field demonstrated a greater capacity to release negative ions [29]. The Fe-free TM in NaCl solution exhibited a zeta potential of −42.9 mV, while the Fe-rich counterpart displayed a more positive value of −21.5 mV. The result indicated a higher density of electrostatic charges on the surface of the Fe-free TM, suggesting a more potent polarization electric field compared to Fe-rich TM (Fig. 3a) [30]. The transient current response of the two TMs was measured with

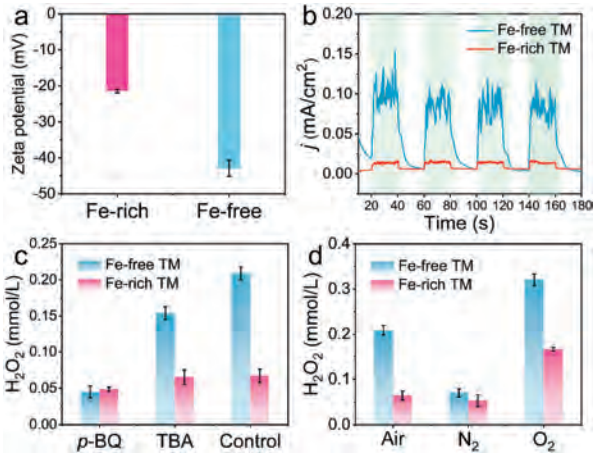


Fig. 3. (a) Zeta potential at pH 7. (b) Transient current response under ultrasonic vibration. (c) Radical-quenching tests. (d) Piezoelectric H_2O_2 generation under different atmospheres over Fe-free and Fe-rich TM. Experimental conditions: Catalysts dosage = 0.4 g/L, ultrasonic power = 100 W, temperature = 25 °C.

ultrasonic vibration both on and off. The Fe-free TM exhibited a significantly higher current intensity compared to the Fe-rich TM, and this result aligned well with H_2O_2 production rate (Fig. 3b). Furthermore, electrochemical impedance spectra (EIS) and liner sweep voltammograms (LSV) were conducted to investigate the separation rate of carriers. EIS analysis revealed a diminished semicircular arc in the Nyquist plot for Fe-free TM compared to Fe-rich TM, indicative of accelerated charge transfer dynamics [31,32]. The experimental data were analysed *via* an equivalent circuit model, as depicted in the inset of Fig. S13 (Supporting information), where R_s, R_{ct}, Q represented the solution resistance, charge transfer resistance value between the electrode and solution, and the electrode double-layer capacitance respectively [33]. The simulated R_{ct} values were shown in Table S1 (Supporting information). As illustrated in Fig. S14 (Supporting information), under a given anode potential, the current density measured over Fe-free TM was higher than that over Fe-rich TM. These results confirmed that Fe-free TM exhibited superior charge transfer rate, demonstrating potential for piezoelectric H_2O_2 production [34,35].

To investigate the pathway of piezoelectric H_2O_2 production, scavengers were used to quench superoxide ($O_2^{\bullet-}$), and hydroxyl radicals ($HO^{\bullet}$) [36,37]. As illustrated in Fig. 3c and Fig. S15 (Supporting information), when $O_2^{\bullet-}$ was inhibited by *p*-benzoquinone (*p*-BQ), the piezoelectric H_2O_2 production experienced a sharp decline over Fe-free TM, whereas only a slight decrease was observed when $HO^{\bullet}$ was scavenged by *tert*–butylalcohol (TBA). Besides, when the atmosphere was switched to O_2, the H_2O_2 production rate increased by 53.4 %, while it decreased by 66.5 % in an N_2 atmosphere (Fig. 3d). Together these results suggested that ORR was the predominant route for piezoelectric H_2O_2 production over Fe-free TM at ambient conditions, while WOR process played a limited role [11]. A similar trend in H_2O_2 production was observed over Fe-rich TM in the scavenging experiment, implying that the same reaction pathway was involved as with Fe-free TM.

Electron paramagnetic resonance experiment was conducted to detect the intermediates during the piezoelectric H_2O_2 production process *via* TMs [38]. 5,5-Dimethyl-1-pyrroline *N*-oxide (DMPO) was used to capture $O_2^{\bullet-}$ and $HO^{\bullet}$ involved in the ORR and WOR process (Fig. S16 in Supporting information) [37]. As shown in Fig. 4a, Fe-free TM displayed a stronger signal corresponding to the DMPO–$O_2^{\bullet-}$ adduct than Fe-rich TM. Notably, a more pronounced signal attributed to DMPO–$HO^{\bullet}$ was detected in the Fe-rich TM system than in the Fe-free system, as illustrated in Fig. 4b and the fitting curves in Fig. S17 (Supporting information), which con-

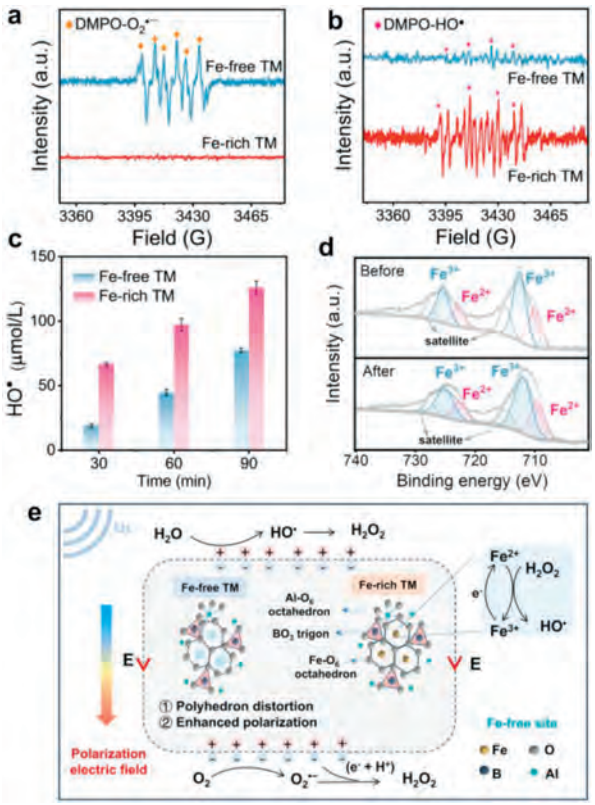


Fig. 4. (a) Spin-trapping EPR spectra of DMPO–$O_2^{\bullet-}$ and (b) DMPO–$HO^{\bullet}$. (c) The concentration of $HO^{\bullet}$ radicals. (d) The corresponding high-resolution XPS spectra of Fe 2p of Fe-rich TM before and after piezocatalytic reaction. (e) The scheme of piezocatalytic H_2O_2 production over Fe-rich TM and Fe-free TM.

trasted with the its comparatively lower H_2O_2 yield. To figure out the immanent cause, the generation of $HO^{\bullet}$ of these two TMs was evaluated by fluorescent probes (Figs. S18 and S19 in Supporting information) [25]. As depicted in Fig. 4c, a higher production of $HO^{\bullet}$ radicals was observed in Fe-rich TM compared to Fe-free TM. Within the first 30 min, Fe-rich TMs generated 66.5 μmol/L of $HO^{\bullet}$, which was 3.5 times higher than Fe-free TM (18.9 μmol/L). It has been previously reported that Fe-containing TM demonstrated an ability to activate H_2O_2 to produce $HO^{\bullet}$ with a high constant reaction rate (k = 40–80 L mol^{-1} s^{-1}) [39–40]. Therefore, the high-resolution XPS spectra of Fe 2p of Fe-rich TM was obtained to analyse the oxidation state distribution of Fe^{2+} and Fe^{3+} before and after piezocatalytic reaction. Gaussian fitting of the peaks, presented in Fig. 4d, showed that the peaks at 709.2 and 722.32 eV before the reaction corresponding to Fe^{2+} in Fe-rich TM, while those at 711.8 and 724.9 eV were associated with Fe^{3+} [18]. After the reaction, the peaks for Fe^{2+} were shifted to 709.5 and 722.6 eV, while the Fe^{3+} peaks moved to 711.9 and 725.1 eV. The Fe^{2+}/Fe^{3+} ratio on the surface of Fe-rich tourmaline was 0.56 before the piezo-catalytic reaction, and remained nearly unchanged at 0.55 afterward (Table S2 in Supporting information). The stable Fe^{2+}/Fe^{3+} ratio suggested that, despite the slow reduction of Fe^{3+} to Fe^{2+} by H_2O_2 (0.001–0.01 L mol^{-1} s^{-1}), the external piezoelectric field effectively facilitated the Fe^{3+}/Fe^{2+} cycling [39].

Based on the above analysis, a logical hypothesis was proposed as follows (Fig. 4e). The removal of Fe from the YO_6 octahedron led to distortion of the polyhedron in the Fe-free TM, resulting in an enhanced polarization that strengthened the electric field at the surface. Under Us vibration, the polarization-induced surface charges facilitated a step-by-step reduction of O_2 to H_2O_2 over Fe-free TM. Concurrently, a water molecule was oxidized by the positive piezoelectric charges to form a $HO^{\bullet}$ radical, and the recom-

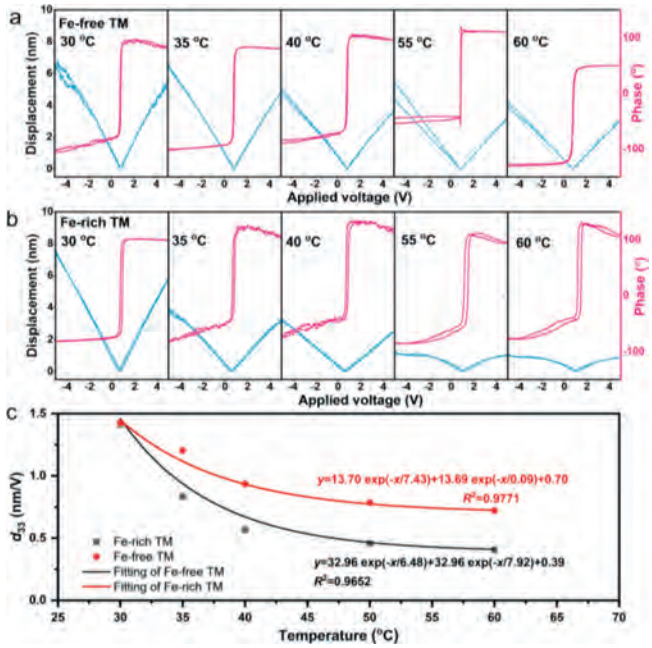


Fig. 5. Piezoresponse force microscopy (PFM) analysis of (a) Fe-free TM and (b) Fe-rich TM under different temperature. (c) Correlation between temperature *versus* d_{33}.

bination of two HO• radicals generated H_2O_2. In the case of Fe-rich TM, the H_2O_2 generation pathway was similar, however, the presence of Fe promoted the dissociation of H_2O_2. The diminished piezoelectric response of the Fe-rich TM, coupled with the catalytic dissociation of H_2O_2 by Fe, resulted in a lower piezoelectric H_2O_2 production rate compared to the Fe-free TM.

Given the temperature increased during the Us vibration process, temperature-dependent PFM was conducted to analyse the relationship between temperature and piezocatalytic activity of these two TMs. The observed ~180° phase-voltage hysteresis loops and the butterfly-shaped amplitude-voltage curves in Figs. 5a and b confirmed the piezoelectric properties of both TMs. Furthermore, the piezocatalytic activity of these two TMs was quantitated by piezoelectric d_{33} coefficient, which can be calculated as [41]:

$$d_{33}=\frac{D-D_I}{V-V_I} \quad (1)$$

where D_I and V_I represent the displacement and voltage, respectively, at the intersection of the loop [33]. D and V are the respective values at different points of the loop. Fig. 5c demonstrated a negative correlation between maximum effective d_{33} coefficients and temperature. Across all temperatures, the d_{33} values of the Fe-free TM were significantly higher than those of the Fe-rich TM, consistent with prior results indicating superior piezoelectric performance in Fe-free TM. As temperature increased, d_{33} decreased for both materials, with Fe-free TM exhibiting a slower decline compared to Fe-rich TM. The superior performance and thermal stability of Fe-free TM made it a promising candidate for applications requiring high and stable piezoelectric properties over a range of temperatures.

In conclusion, piezo-catalytic H_2O_2 synthesis was effectively accomplished using two natural tourmalines. Compared to Fe-rich TM, Fe-free TM exhibited superior piezo-catalysis activity. In-depth analysis unveiled the underlying mechanism of H_2O_2 generation pathway indicating that ORR processes predominantly contributed to H_2O_2 production while the presence of Fe promoted the dissociation of H_2O_2 into HO• radicals. The removal of Fe from the YO_6 octahedron in Fe-free TM induced polyhedral distortion, which significantly enhanced the polarization within the catalysts. The increased polarization amplified the surface electric field, strengthening the piezoelectric effect and improving the piezo-catalytic performance. This work provides new insight into the mechanisms of piezoelectric H_2O_2 production by natural tourmaline.

Declaration of competing interest

The authors declare that they have no known competing financial interests or personal relationships that could have appeared to influence the work reported in this paper.

CRediT authorship contribution statement

Huiru Chen: Writing – original draft, Methodology, Investigation, Formal analysis. **Zhi Li:** Writing – review & editing, Supervision, Conceptualization. **Jingyi Yang:** Methodology, Investigation. **Li Gong:** Writing – review & editing, Supervision. **Mingshan Zhu:** Project administration, Funding acquisition.

Acknowledgments

This work has been supported by the National Natural Science Foundation of China (Nos. 22322604 and 22506055). This work is thankful to Dr. Xiang Yu, from the Analytical and Testing Center of Jinan University for providing technical supports.

Supplementary materials

Supplementary material associated with this article can be found, in the online version, at doi:10.1016/j.cclet.2025.111743.

References

[1] C. Xia, Y. Xia, P. Zhu, et al., Science 366 (2019) 226–231.
[2] Y. Bu, Y. Wang, G.F. Han, et al., Adv. Mater. 33 (2021) 2103266.
[3] Q. Wu, J. Cao, X. Wang, et al., Nat. Commun. 12 (2021) 483.
[4] S. Yang, A. Verdaguer-Casadevall, L. Arnarson, et al., ACS Catal. 8 (2018) 4064–4081.
[5] Y. Zhou, H. Dong, Z. Xu, et al., Appl. Catal. B: Environ. 343 (2024) 123504.
[6] C. Liu, J. Zhang, W. Wang, et al., Surf. Interfaces 42 (2023) 103491.
[7] H. Chen, R. Yin, M. Zhu, Water Res. 274 (2025) 123026.
[8] J. Liu, W. Qi, M. Xu, et al., Angew. Chem. Int. Ed. 62 (2023) e202213927.
[9] S. Sun, J. Li, H. Ding, et al., Chem. Eng. J. 460 (2023) 141718.
[10] K. Wang, Z. Guan, Y. He, M. Fan, Nano Energy 133 (2025) 110518.
[11] Z. Li, H. Lv, K. Tong, et al., Appl. Catal. B: Environ. Energy 345 (2024) 123690.
[12] J. Teng, W. Li, Z. Wei, et al., Angew. Chem. Int. Ed. 63 (2024) e202416039.
[13] J. Li, X. Liu, G. Zhao, et al., Sci. Total Environ. 869 (2023) 161767.
[14] Z. Li, S. Lan, M. Zhu, Environ. Sci. Ecotechnol. 18 (2024) 100329.
[15] X. Yu, Z. Wei, Y. Qin, et al., Adv. Mater. 37 (2025) 2501494.
[16] Y. Liang, X. Tang, Q. Zhu, et al., Chemosphere 281 (2021) 130780.
[17] B. Niu, N. Wang, Y. Chen, et al., Sep. Purif. Technol. 257 (2021) 117893.
[18] D. Wang, H. Xu, J. Ma, et al., Chem. Eng. J. 354 (2018) 113–125.
[19] T. Yu, J. Wang, N. Ding, et al., J. Ind. Eng. Chem. 131 (2024) 44–53.
[20] H. Zhao, Z. Zheng, S. Zhu, et al., Chem. Eng. J. 477 (2023) 147094.
[21] A.V. Spivak, E.Y. Borovikova, T.V. Setkova, Spectrochim. Acta Part A 248 (2021) 119171.
[22] A. Ertl, J.M. Hughes, F. Pertlik, et al., Can. Mineral. 40 (2002) 153–162.
[23] C. Zhao, D. Zhang, L. Liao, X. Sun, J. Chin, Ceram. Soc. 36 (2008) 854–857.
[24] C. Feng, L. Tang, Y. Deng, et al., Adv. Funct. Mater. 30 (2020) 2001922.
[25] X.F. Li, A. Berbille, T.Y. Wang, et al., Adv. Funct. Mater. 34 (2024) 2315817.
[26] G. Zhang, X. Qin, Mater. Res. Bull. 48 (2013) 3743–3749.
[27] G. Li, D. Chen, W. Zhao, X. Zhang, J. Environ. Chem. Eng. 3 (2015) 515–522.
[28] H. He, F. Duan, X. Liu, et al., J. Alloys Compd. 999 (2024) 175019.
[29] J. Liu, Y. Qin, S. Yuan, et al., J. Mol. Liq. 332 (2021) 115854.
[30] S.M. Chang, S. Hur, J. Park, et al., Addit. Manuf. 67 (2023) 103470.
[31] A.Y. Zha, Q.B. Zha, Z. Li, et al., Rare Met. 42 (2022) 1274–1282.
[32] X. Zhou, K. Wang, Y. Wang, et al., Langmuir 40 (2024) 11251–11262.
[33] Y. Li, Z. Li, X. Lin, et al., Chem. Commun. 59 (2023) 5749–5752.
[34] Y. Zhou, Z. Xu, L. Tang, et al., Environ. Sci. Technol. 58 (2024) 6049–6057.
[35] W. Wei, Z. Wei, R. Li, et al., Green Carbon 2 (2024) 291–299.
[36] Y. Chen, J. Kang, Z. Li, et al., Surf. Interfaces 40 (2023) 103045.
[37] M. Zhang, W. Guo, Y. Chen, et al., Chin. Chem. Lett. 34 (2023) 108229.
[38] J. He, Z. Li, P. Feng, et al., Angew. Chem. Int. Ed. 63 (2024) e202410381.
[39] Y. Zhu, J. Zhu, H. ShenTu, et al., Appl. Catal. B: Environ. 334 (2023) 122824.
[40] X. Zhai, Z. Wei, Z. Lu, et al., Adv. Funct. Mater. 35 (2025) 2503667.
[41] Z. Li, Y. Zhou, Y. Zhou, et al., Nat. Commun. 14 (2023) 5742.